ARTICLE

Crystallographic and Morphological Sensitivity of N_2 Activation over Ruthenium

Hao Lin[a, d†], Jin-xun Liu[b†], Hong-jun Fan[a*], Wei-xue Li[b, c*]

a. State Key Laboratory of Molecular Reaction Dynamics, Dalian Institute of Chemical Physics, Chinese Academy of Science, Dalian 116023, China
b. Department of Chemical Physics, School of Chemistry and Materials Science, University of Science and Technology of China, Hefei 230026, China
c. Hefei National Laboratory for Physical Science at the Microscale, iCHEM, University of Science and Technology of China, Hefei 230026, China
d. University of Chinese Academy of Sciences, Beijing 100049, China

(Dated: Received on September 25, 2020; Accepted on November 17, 2020)

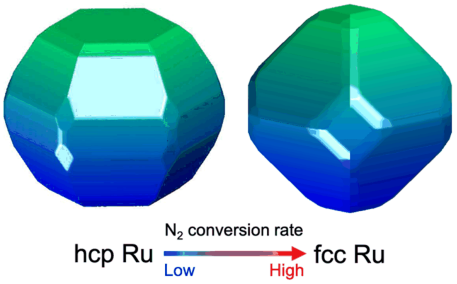

Ruthenium (Ru) serves as a promising catalyst for ammonia synthesis via the Haber-Bosch process, identification of the structure sensitivity to improve the activity of Ru is important but not fully explored yet. We present here density functional theory calculations combined with microkinetic simulations on nitrogen molecule activation, a crucial step in ammonia synthesis, over a variety of hexagonal close-packed (hcp) and face-center cubic (fcc) Ru facets. Hcp $\{21\bar{3}0\}$ facet exhibits the highest activity toward N_2 dissociation in hcp Ru, followed by the monatomic step sites. The other hcp Ru facets have N_2 dissociation rates at least three orders lower. Fcc $\{211\}$ facet shows the best performance for N_2 activation in fcc Ru, followed by $\{311\}$, which indicates stepped surfaces make great contributions to the overall reactivity. Although hcp Ru $\{21\bar{3}0\}$ facet and monatomic step sites have lower or comparable activation barriers compared with fcc Ru $\{211\}$ facet, fcc Ru is proposed to be more active than hcp Ru for N_2 conversion due to the exposure of the more favorable active sites over step surfaces in fcc Ru. This work provides new insights into the crystal structure sensitivity of N_2 activation for mechanistic understanding and rational design of ammonia synthesis over Ru catalysts.

Key words: Ammonia synthesis, N_2 activation, Density functional theory, Ru, Crystallographic and morphological sensitivity

I. INTRODUCTION

Ammonia synthesis via Haber-Bosch process has played a crucial role in the development of the chemical industry during the 20th century [1, 2]. Industrially, the Haber-Bosch process is mainly operated at elevated temperature and pressure [3, 4], typically catalyzed by Fe [5−10] and Ru [11−16] catalysts. Due to the broad range of applications and the vital importance, the synthesis of ammonia is probably the most extensively studied reaction in heterogeneous catalysis [17, 18]. A large number of experimental and theoretical studies have been devoted to elucidating the reaction mechanism and identifying the active sites of ammonia synthesis reaction [19−23]. It has been well established that dissociative chemisorption of N_2 is particularly structure-sensitive and N_2 dissociation is often considered as the rate-determining step over Fe and Ru catalysts [16, 24−28]. Deeper insight into the structure sensitivity and active site distribution of N_2 activation is a significant way to improve particularly the mass-specific activity of Ru with economic efficiency.

The structure sensitive N_2 activation and ammonia synthesis were studied extensively before, mainly on hexagonal close-pack (hcp) Ru [29]. Surface experiments combined with the density functional theory (DFT) calculations showed that ammonia synthesis over Ru should also be a very structure-sensitive reac-

†These authors contributed equally to this work.
*Authors to whom correspondence should be addressed. E-mail: wxli70@ustc.edu.cn, fanhj@dicp.ac.cn

DOI:10.1063/1674-0068/cjcp2009171 ©2020 Chinese Physical Society

tion [12, 13], even more obviously than on Fe. Dahl *et al.* showed that the dissociative chemisorption of nitrogen over Ru (0001) surface are dominated by the so-called B_5 sites located at the surface steps [30]. N_2 adsorption/desorption rates at the terraces are several orders of magnitude lower than that at the step B_5 sites [13]. Therefore, B_5 sites were proposed active for N_2 dissociation on Ru nanoparticles, which has a maximum NH_3 synthesis activity at 2 nm [18]. Raróg-Pilecka *et al.* showed that the turnover frequency of NH_3 synthesis increased as the particle size increased from 0.7 nm to 4 nm. Extrapolation to lower sizes indicates that Ru crystallites smaller than 0.7−0.8 nm might be totally inactive [28], due to the lack of B_5 sites which is not available at small size otherwise. However, Kim *et al.* demonstrated that the sites presented on a double-stepped Ru (109) surface are relatively more active than the stepped Ru (0001) surface [31]. Shetty *et al.* studied Ru ($11\bar{2}1$) surface can be active for N_2 dissociation [32]. Recently, N_2 activation was studied over a variety of planar Ru (0001), quasi-planar ($10\bar{1}1$) step and edge sites by DFT calculations, and in addition to B_5 sites, several competitive edge sites were found and could contribute to the overall reactivity [33]. Despite extensive investigations so far, only few representative surfaces together with corresponding step/edge sites are considered. For supported hcp Ru nanoparticles, the exposed sites are highly heterogeneous and their structure sensitivity as well as contributions to the overall activity for N_2 activation remains open.

The impact of crystal structures on chemical reactions, in addition to morphology, has attracted much attention and been widely investigated in recent years [34−49]. For example, experiments found that hcp cobalt (Co) exhibits higher activity than face-center cubic (fcc) Co for Fischer-Tropsch synthesis (FTS) process [50−54]. DFT calculations revealed that hcp Co is significantly more active than fcc Co for CO and N_2 activation, due to the sites available not only with lower barrier but also with higher abundance over hcp Co [55, 56]. On the other hand, fcc Ru was predicted to have a higher mass-specific activity for CO dissociation than hcp Ru for exposing the abundant sites though corresponding barriers were not the lowest one. Theoretical prediction was verified by subsequent experiment, where the synthesized fcc Ru shows extraordinary higher mass-specific activity than hcp Ru in FTS [46]. For N_2 activation on fcc Ru, fcc Ru (111) and (001) surfaces were found to be more active than hcp Ru (0001) surface [57]. Whether and why the overall activity for N_2 activation on fcc Ru is higher than hcp Ru was not studied yet.

To address the above questions, N_2 activation on hcp Ru and fcc Ru was thoroughly investigated by DFT study in this work. Structure sensitivity were explored in depth by considering a number of facets in both hcp Ru and fcc Ru, and exposed facets and corresponding morphologies were determined by Wulff construction based on the calculated surface energies. N_2 activation was studied over all the exposed facets in the hcp Ru and fcc Ru Wulff shapes, and corresponding dissociation rate and conversion rate taking into account of the site distribution were calculated. The crystal structure sensitivity of hcp Ru and fcc Ru along with rational design for more effective Ru-based catalysts for N_2 dissociation and ammonia synthesis were discussed finally.

II. COMPUTATIONAL DETAILS

All the DFT calculations were performed by using the Vienna *ab initio* simulation package (VASP) [58, 59]. Projector augmented wave potentials [60] and the generalized gradient approximation with the Perdew-Burke-Ernzerhof exchange-correlation functionals [61] were adopted. The plane wave cutoff energy was specified by 400 eV and the convergence threshold for geometry optimizations was set to 10^{-4} eV. When all the forces on the atoms are less than 0.01 eV/Å, the geometry optimizations are considered to be converged. Monkhorst-Pack [62] mesh k-points samplings of (12×12×1) and (10×10×1) were used for the bulk hcp Ru and fcc Ru calculations, respectively. The optimized lattice constants of hcp Ru are a=2.728 Å and c/a=1.575, which are in good agreement with the experimental values of a=2.70 Å and c/a=1.582 [63]. The calculated lattice constant fcc Ru was 3.818 Å, in line with the experimental measurement [64].

The p(2×2) slab models of hcp Ru and fcc Ru surfaces usually have metal layers of 6−9 Å thickness. The stepped hcp Ru (0001) surface was modeled by a p(3×4) slab with removing two rows Ru atoms on the surface. Neighboring slabs are separated by a vacuum of 15 Å, to avoid the interactions between them. We took the fcc Ru (111) surface as an example to describe the computational details. The Ru (111) surface was modeled with a four-layers slab, the bottom two layers were constrained at their bulk positions, and the top two Ru layers and adsorbed molecules were allowed to relax. All the other hcp Ru and fcc Ru surfaces were simulated by slabs resemble to four (111) layers thickness and relaxation constraints with the k-point density keeping at ∼0.03/Å for all the slab calculations.

For a given surface, the adsorption energy is calculated as:

$$E_{\rm ads} = E_{\rm ads/slab} - E_{\rm slab} - E_{\rm gas} \quad (1)$$

where, $E_{\rm ads/slab}$, $E_{\rm slab}$ and $E_{\rm gas}$ are the total energies of Ru surface with an adsorbate, clean Ru surface, and corresponding gaseous molecule and radical, respectively.

The force reversed method [65] was used to determine the transition states (TS) within a force tolerance of 0.03 eV/Å. Some of the identified transition states were also characterized again by using the climbing-image nudged elastic band method (CI-NEB) [66] implemented in VASP to reaffirm the identified TS. Fre-

DOI:10.1063/1674-0068/cjcp2009171 ©2020 Chinese Physical Society

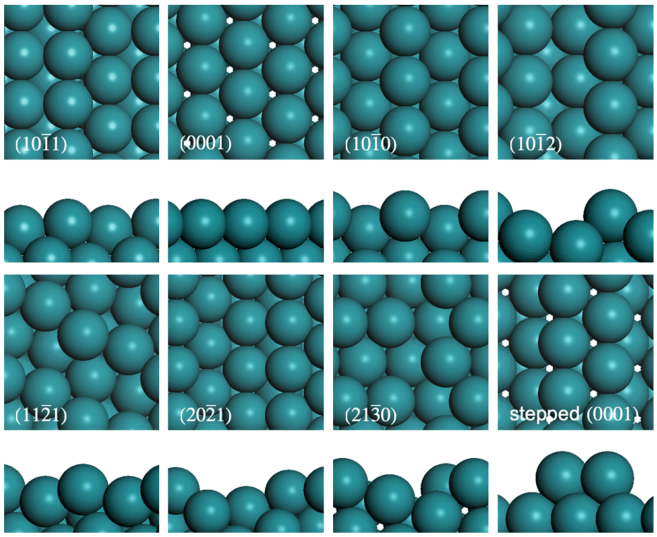

FIG. 1 Top and side view of bare hcp Ru surfaces.

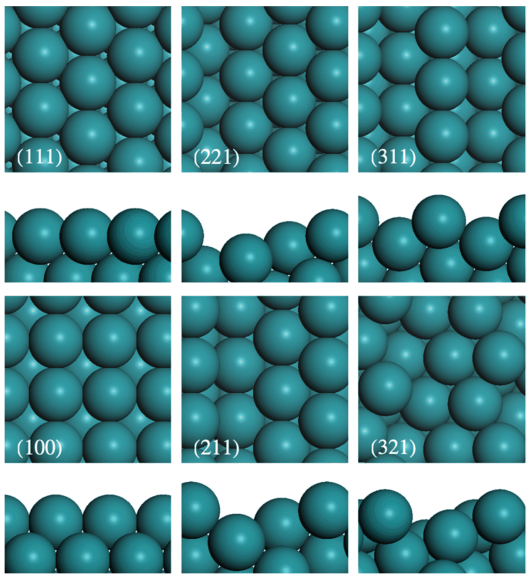

FIG. 2 Top and side view of bare fcc Ru surfaces.

quency analysis confirmed that all the located TS have only one imaginary frequency. We adopt the adsorbed N_2 molecules and the separated N atom in their most stable adsorption site as the initial and final states for N_2 activation, respectively.

III. RESULTS AND DISCUSSION

A. Morphologies of hcp Ru and fcc Ru

The thermodynamic equilibrium shapes of hcp Ru and fcc Ru can be obtained by the Wulff construction based on the calculated surface energies [67]. The Wulff shapes and corresponding surface area proportions of the exposed surfaces in hcp Ru and fcc Ru were presented in our previous work [68], and FIGs. 1 and 2 show the top view and side view of all the clean surfaces considered in the present work. Obviously, the differences in stacking sequence and point group symmetries result in different morphologies between hcp Ru and fcc Ru [69].

The morphologies of hcp Ru and fcc Ru are dihedral-like and octahedron-like shapes, respectively. From our previous work, we have found that {0001} facets have the highest stability, followed by {10$\bar{1}$1}, {10$\bar{1}$0}, {20$\bar{2}$1}, {10$\bar{1}$2}, {11$\bar{2}$1}, and {21$\bar{3}$0} facets for hcp Ru with the surface energies of 160, 177, 181, 184, 188, 200 and 202 meV/Å^2, respectively. The surface area of a specific facet is determined by not only the surface energy but also the orientations. {10$\bar{1}$1} facets group has the highest surface area proportion in hcp Ru Wulff shape with a value of 54%. Whereas {0001} (18%), {10$\bar{1}$0} (16%) and {10$\bar{1}$2} (6%) facets cover the remaining morphology of hcp Ru dominantly. High-index corrugated facets are less exposed in hcp Ru morphology due to their high surface energies. Specifically, {11$\bar{2}$1}, {20$\bar{2}$1}, and {21$\bar{3}$0} facets have the surface area proportion of 4%, 2% and 1%, respectively. Our predicted thermodynamic equilibrium morphology of hcp Ru is slightly different from that given by Nørskov *et al.* [18], which may originate from the calculated surface energies discrepancy caused by different potentials and exchange-correlation functionals.

When coming to fcc Ru, the exposed facets in fcc Ru Wulff shape are often {111}, {221}, {211}, {321}, {311} and {100} with the surface energies of 145, 163, 172, 174, 180, and 184 meV/Å^2, respectively. In contrast to the flat {0001} surface in hcp Ru Wulff morphology, the close-packed {111} surface in fcc Ru has the lowest surface energy and takes as large as 63% of the total surface area in the fcc Ru Wulff shape, followed by {221} (14%), {311} (9%), {100} (6%), {211} (4%), and {321} (3%), respectively. N_2 activation was studied over all the exposed facets in hcp Ru and fcc Ru bellow to identify their crystallographic structure effect and structure-sensitivity relationship.

B. N_2 and N adsorption

First of all, we studied the chemisorption of N_2 molecule and N atom at various high-symmetry sites of each facet exposed in the Wulff shapes of hcp Ru and fcc Ru. The energetic and geometric information for N_2 molecules and N atoms adsorption over various hcp Ru and fcc Ru facets are listed in Table I. The corresponding most stable N atom adsorption configurations over hcp Ru and fcc Ru facets are shown in FIG. 3 and FIG. 4, respectively. N_2 molecule always prefers to bind perpendicularly to the topmost layered Ru atoms over all the hcp Ru and fcc Ru facets. The calculated N_2 ad-

DOI:10.1063/1674-0068/cjcp2009171 ©2020 Chinese Physical Society

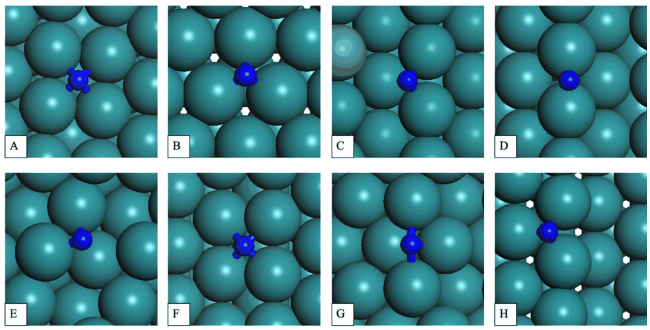

FIG. 3 Top view of N atom adsorbed on hcp Ru surfaces: (A) $(10\bar{1}1)$, (B) (0001) (C) $(10\bar{1}0)$, (D) $(10\bar{1}2)$, (E) $(11\bar{2}1)$, (F) $(20\bar{2}1)$, (G) $(21\bar{3}0)$, (H) stepped (0001). The blue and cyan spheres represent the N and Ru atoms, respectively, and is used throughout this paper.

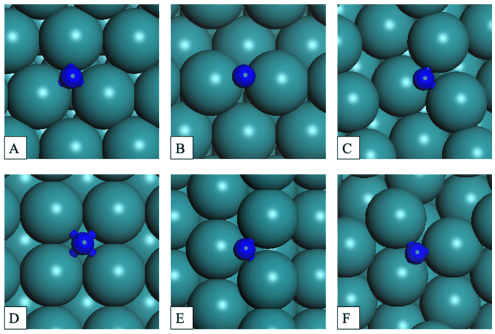

FIG. 4 Top view of N atom adsorbed on fcc Ru surfaces: (A) (111), (B) (221), (C) (311), (D) (100), (E) (211), (F) (321).

TABLE I Adsorption energy ($E_{N_2}^{ads}$ and E_N^{ads}, eV) of N_2 and N with respect to the corresponding gaseous molecule and radical, the selected adsorption geometric parameters ($d_{N\text{-}N}$, Å) for the most stable N_2 and N atom adsorption site on hcp and fcc Ru surfaces.

Facet		$E_{N_2}^{ads}$	$d_{N\text{-}N}$	E_N^{ads}	Adsorption site
hcp	$(10\bar{1}1)$	−0.72	1.135	−6.20	4-fold
	(0001)	−0.61	1.135	−6.03	hcp-hollow
	$(10\bar{1}0)$	−0.85	1.137	−5.82	3-fold
	$(10\bar{1}2)$	−0.70	1.136	−5.92	bridge
	$(11\bar{2}1)$	−0.79	1.137	−5.95	3-fold
	$(20\bar{2}1)$	−0.85	1.136	−6.15	4-fold
	$(21\bar{3}0)$	−0.92	1.139	−5.98	4-fold
	Stepped (0001)	−0.86	1.138	−5.79	hcp-hollow
fcc	(111)	−0.61	1.136	−6.30	hcp-hollow
	(221)	−0.76	1.137	−5.96	bridge
	(311)	−0.80	1.138	−6.08	edge-hcp
	(100)	−0.71	1.136	−6.34	4-fold
	(211)	−0.86	1.138	−6.36	edge-hcp
	(321)	−0.85	1.137	−6.36	edge-hcp

sorption energies ($E_{N_2}^{ads}$) vary from −0.61 eV/(0001) to −0.92 eV/$(21\bar{3}0)$ for hcp Ru and from −0.61 eV/(111) to −0.86 eV/(211) for fcc Ru facets. Generally, N_2 molecule adsorbs weaker on close-packed hcp Ru (0001) and fcc Ru (111) surface than those on the other corrugated facets containing more unsaturated surface Ru atoms. The overall variation of N_2 adsorption energies among different facets are 0.31 eV for hcp Ru and 0.25 eV for fcc Ru, indicating less structure sensitivity.

Different from N_2 adsorption, N atom prefers to coordinate with more surface Ru atoms (Table I, FIG. 3, and FIG. 4). N adsorption is structurally more sensitive as compared with N_2 adsorption. N atom adsorption energies vary from −5.79 eV to −6.20 eV for hcp Ru and from −5.96 eV to −6.36 eV for fcc Ru. Specifically, N atom adsorbs strongly at the 4-fold sites of $(10\bar{1}1)$, $(20\bar{2}1)$ and $(21\bar{3}0)$ facets with the adsorption energies of −6.20, −6.15 and −5.98 eV, respectively. Whilst N atom adsorbs at the 3-fold site which is less favorable over (0001) (−6.03 eV), $(11\bar{2}1)$ (−5.95 eV), $(10\bar{1}0)$(−5.82 eV) and stepped (0001) (−5.79 eV) facets. However, N atom is more likely to adsorb at the bridge site on $(10\bar{1}2)$ surface with an adsorption energy of −5.92 eV. For fcc Ru surfaces, N atom adsorbs favorably at the edge-hcp site of (211), (321) and (311) facets with the adsorption energies of −6.36, −6.36 and −6.08 eV, respectively. On (111) and (100) surface, N atom has nearly the same adsorption energies (−6.30 eV *vs.* −6.34 eV) at hcp-hollow and 4-fold sites, respectively. N atom adsorbs the weakest at the bridge site over the (221) facet with an adsorption energy of −5.96 eV. In a word, N atom adsorbs stronger on most of the fcc Ru facets than on hcp Ru $(10\bar{1}1)$ facet which binds N atom strongest among all the exposed facets in hcp Ru Wulff shape. The adsorption energy of N atom increases with the coordination number of N atom binding to the surface Ru atoms. N adsorption strength follows the sequence at the adsorption site of 4-fold>3-fold>bridge site. The large variation of N_2 and N adsorption energies among different hcp Ru and fcc Ru facets will result in a great structure sensitivity of N_2 activation.

C. N_2 Dissociation

N_2 activation is systematically studied over all the exposed facets in the Wulff shapes of hcp Ru and fcc Ru. Activation barrier and the reaction enthalpy of N_2 dissociation with respect to N_2 at their most stable adsorption site are shown in Table II. The TS configurations are given in FIG. 5 and FIG. 6 for hcp Ru and fcc Ru, respectively.

N_2 dissociation reaction is highly exothermic and the reaction energies vary greatly among different hcp Ru and fcc Ru facets. Reaction energy of N_2 activation is determined by both the N_2 and N atom adsorption energies. The reaction energies for N_2 activation vary from −0.41 eV/$(10\bar{1}0)$ to −1.29 eV/$(10\bar{1}1)$

DOI:10.1063/1674-0068/cjcp2009171 ©2020 Chinese Physical Society

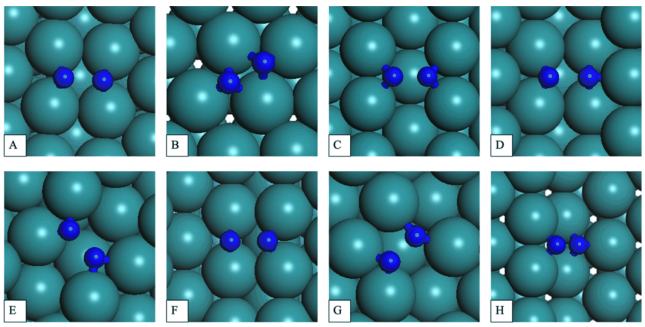

FIG. 5 Top view of N_2 dissociation TS structures on hcp Ru surfaces: (A) $(10\bar{1}1)$, (B) (0001), (C) $(10\bar{1}0)$, (D) $(10\bar{1}2)$, (E) $(11\bar{2}1)$, (F) $(20\bar{2}1)$, (G) $(21\bar{3}0)$, (H) stepped (0001).

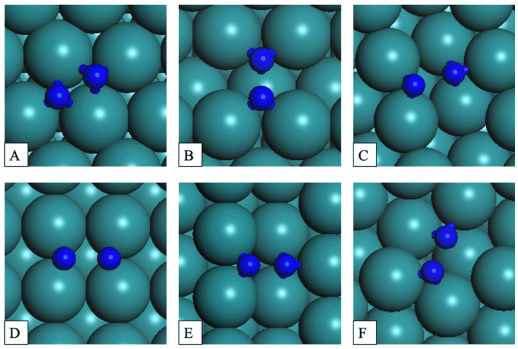

FIG. 6 Top view of N_2 dissociation TS structures on fcc Ru surfaces: (A) (111), (B) (221), (C) (311), (D) (100), (E) (211), (F) (321).

TABLE II Calculated activation energies (E_a, in eV), reaction energies (ΔH, in eV) with respect to N_2 at their most stable adsorption state, and the distance between the two N atoms ($d_{N\text{-}N}$, in Å) at TS for N_2 dissociation reaction on hcp Ru and fcc Ru surfaces.

Facet		E_a/eV	ΔH/eV	$d_{N\text{-}N}$/Å
hcp	$(10\bar{1}1)$	1.03	−1.29	1.861
	(0001)	1.69	−1.07	1.726
	$(10\bar{1}0)$	1.22	−0.41	1.700
	$(10\bar{1}2)$	1.25	−0.77	1.898
	$(11\bar{2}1)$	1.05	−0.73	1.818
	$(20\bar{2}1)$	1.18	−1.07	1.890
	$(21\bar{3}0)$	0.77	−0.67	1.857
	Stepped (0001)	0.82	−0.35	1.823
fcc	(111)	1.38	−1.60	1.694
	(221)	1.05	−0.79	1.797
	(311)	1.01	−0.99	1.895
	(100)	0.97	−1.59	1.900
	(211)	0.81	−1.48	1.849
	(321)	1.19	−1.49	1.867

for hcp Ru facets, whereas from −0.79 eV/(221) to −1.60 eV/(111) for fcc Ru facets. The activation barriers for N_2 dissociation were calculated to be in the region of 0.77 eV/$(21\bar{3}0)$−1.69 eV/(0001) for all the hcp Ru facets including the stepped (0001) surface and 0.81 eV/(211)−1.38 eV/(111) for the fcc Ru facets. On the close-packed hcp Ru (0001) and fcc Ru (111) facets, the two N atoms are located at the fcc and hcp hollow site at the TS of N_2 dissociation, which is consistent with Crawford and Hu's findings [70]. Since two N atoms share two surface Ru metal atoms at the TS of N_2 dissociation, the large repulsive interaction between them gives rise to the highest N_2 dissociation barrier among all the hcp Ru and fcc Ru surfaces. Subsequently, the calculated N_2 activation barriers are 1.69 eV for hcp Ru (0001) and 1.38 eV for fcc Ru (111). Two N atoms sharing one Ru atom at TS decreases N_2 dissociation barrier to 1.22 eV on the hcp Ru $(10\bar{1}0)$ surface. Whereas on the hcp Ru $(10\bar{1}1)$, $(20\bar{2}1)$, stepped (0001) and fcc Ru (100) facets, the two N atoms are located at the bridge sites in TS without sharing any Ru atoms, which results in the N_2 dissociation barrier lower by more than 0.04 eV. Whereas, on the other hcp and fcc Ru facets, one N atom sits at the 3-fold site and the other N atom moves to the bridge site in the TS without sharing Ru atoms, which will even lower the N_2 dissociation barrier. Specifically, the calculated N_2 dissociation barriers are 1.05, 0.77, 1.05, 1.01, 0.81 and 1.19 eV on hcp Ru $(11\bar{2}1)$ and $(21\bar{3}0)$, fcc Ru (221), (311), (211) and (321) facets, respectively. It is obvious that N_2 dissociation reaction is structure sensitive and hcp Ru $(21\bar{3}0)$ and fcc Ru (211) surfaces have the highest activity (the lowest barrier) for N_2 dissociation reaction in hcp Ru and fcc Ru, respectively.

D. Micro-kinetic model for N_2 dissociation

To compare N_2 dissociation activities of hcp Ru and fcc Ru quantitatively, we have performed micro-kinetic simulation. By using the calculated energetics, N_2 dissociation and conversion rates on each facet exposed in hcp Ru and fcc Ru Wulff shapes are computed. Here, we assume N_2 dissociation on Ru surfaces obeying Langmuir-Hinshelwood (L-H) mechanism. N_2 molecules first chemisorb on Ru surface, and then adsorb N_2 molecule, dissociate into two N atoms:

$$N_2 + {}^* \underset{k_{-1}}{\overset{k_1}{\longleftrightarrow}} N_2^* \tag{2}$$

$$N_2^* + {}^* \xrightarrow{k_2} 2N^* \tag{3}$$

Assuming N_2 adsorption process is very fast compared to dissociation so that N_2 adsorption and desorption are in equilibrium. The equilibrium constant K for N_2 adsorption is the ratio of the forward rate constant k_1 to the backward rate constant (k_{-1}):

$$K = \frac{k_1}{k_{-1}} = \frac{\theta_{N_2}}{\theta_* P_{N_2}} = \frac{K^0}{P_0} \tag{4}$$

DOI:10.1063/1674-0068/cjcp2009171 ©2020 Chinese Physical Society

TABLE III Equilibrium constant (K, in Pa^{-1}), reaction rate constant (k_2, in s^{-1}), reaction rate (r, in molecule·site^{-1}·s^{-1}), active site number of 1 m^2 Ru catalysts (N_{act}) and conversion rate (C, in molecule·s^{-1}) for N_2 dissociation process on hcp and fcc Ru surfaces.

	Facet	K	k_2	r	N_{act}	C
hcp Ru	$(10\bar{1}1)$	2.5×10^{-10}	3.8×10^{5}	2.4×10^{2}	4.0×10^{18}	9.5×10^{20}
	(0001)	4.0×10^{-11}	6.8×10^{0}	6.8×10^{-4}	2.8×10^{18}	1.9×10^{15}
	$(10\bar{1}0)$	2.1×10^{-9}	1.7×10^{4}	8.7×10^{1}	1.4×10^{18}	1.2×10^{20}
	$(10\bar{1}2)$	1.8×10^{-10}	1.0×10^{4}	4.4×10^{0}	3.4×10^{17}	1.5×10^{18}
	$(11\bar{2}1)$	7.9×10^{-10}	2.8×10^{5}	5.4×10^{2}	1.9×10^{17}	1.0×10^{20}
	$(20\bar{2}1)$	2.1×10^{-9}	3.2×10^{4}	1.7×10^{2}	8.2×10^{16}	1.4×10^{19}
	$(21\bar{3}0)$	6.8×10^{-9}	2.9×10^{7}	4.7×10^{5}	3.2×10^{16}	1.5×10^{22}
	Stepped (0001)	2.5×10^{-9}	1.3×10^{7}	7.7×10^{4}		
fcc Ru	(111)	4.0×10^{-11}	1.2×10^{3}	1.2×10^{-1}	1.0×10^{19}	1.2×10^{18}
	(221)	4.8×10^{-10}	2.8×10^{5}	3.3×10^{2}	6.4×10^{17}	2.1×10^{20}
	(311)	9.3×10^{-10}	5.4×10^{5}	1.2×10^{3}	7.4×10^{17}	9.2×10^{20}
	(100)	2.1×10^{-10}	1.0×10^{6}	5.4×10^{2}	8.2×10^{17}	4.4×10^{20}
	(211)	2.5×10^{-9}	1.5×10^{7}	9.1×10^{4}	2.2×10^{17}	2.0×10^{22}
	(321)	2.1×10^{-9}	2.7×10^{4}	1.4×10^{2}	1.1×10^{17}	1.6×10^{19}

where θ_{N_2} and θ_* stand for the surface coverages of N_2 molecules and free sites on the Ru surface, respectively. P_{N_2} and P_0 are the partial pressure of N_2 gas and the stand pressure, respectively. N_2 dissociation (Eq.(3)) is irreversible and it is the rate-determining step for ammonia synthesis. Therefore, the surface coverages of N_2 molecule and free active sites obey the sum rule:

$$\theta_{N_2} + \theta_* = 1 \tag{5}$$

Combining Eq.(4) and Eq.(5), we can obtain:

$$\theta_{N_2} = \frac{KP_{N_2}}{1 + KP_{N_2}} \tag{6}$$

$$\theta_* = \frac{1}{1 + KP_{N_2}} \tag{7}$$

Principally, K^0 can be calculated as follows:

$$K^0 = \mathrm{e}^{-\Delta G^0/k_B T} \tag{8}$$

Where ΔG^0 is the change of the stand Gibbs free energy for N_2 adsorption:

$$\begin{aligned}\Delta G^0 &= E_{N_2/slab}(T, P_0) - E_{slab}(T, P_0) - \mu_{N_2}(T, P_0) \\ &\approx E_{N_2/slab}(0\ \mathrm{K}, P_0) - E_{slab}(0\ \mathrm{K}, P_0) - \\ &\quad [E_{N_2}(0\ \mathrm{K}, P_0) + \Delta\mu_{N_2}(T, P_0)] \\ &= E_{N_2}^{ads} - \Delta\mu_{N_2}(T, P_0)\end{aligned} \tag{9}$$

where $E_{N_2}^{ads}$ is the adsorption energy of the N_2 molecule. $E_{N_2/slab}(0\ \mathrm{K}, P_0)$, $E_{slab}(0\ \mathrm{K}, P_0)$ and $E_{N_2}(0\ \mathrm{K}, P_0)$ are the total energies of N_2 adsorption on the Ru surface system, clean slab surface and gaseous N_2 molecule, respectively. While $\mu_{N_2}(T, P_0)$ stands for the standard chemical potentials of N_2 in the gas phase. In order to obtain $\Delta\mu_{N_2}(T, P_0)$, entropy and enthalpy changes were taken from JANAF tables [71], as shown in the following equation

$$\begin{aligned}\Delta\mu_{N_2}(T, P_0) = H(T, P_0) - H(0\,\mathrm{K}, P_0) - \\ TS(T, P_0)\end{aligned} \tag{10}$$

Industrial ammonia synthesis conditions (T=700 K, P=100 bar, N_2 to H_2 ratio of 1:3, with 1%NH_3) were considered in our microkinetic simulations. Subsequently, $\Delta\mu_{N_2}$(700 K, 1 bar)=−1.36 eV was applied in this work.

By using Eq.(3), N_2 dissociation reaction rate can be written as

$$r = k_2\theta_{N_2}\theta_* = \frac{k_2 KP_{N_2}}{1 + KP_{N_2}} \tag{11}$$

The reaction rate constant k_2 can be given by:

$$k_2 = A\mathrm{e}^{-E_a/k_B T} \tag{12}$$

Here, A is the pre-factor, E_a denotes the N_2 activation barrier and k_B is the Boltzmann constant. In order to estimate the reaction rate, we denoted the value of pre-factor A to be 10^{13} s^{-1}. Assuming all the active sites can be used for activating N_2, thus if we consider the total surface area of Ru nanoparticles to be 1 m^2, N_{act} represents the number of the active sites, N_2 conversion rate C of a specified surface can be calculated as:

$$C = N_{act} \times r \tag{13}$$

Combining the above equations, we can derive the N_2 reaction rate constants and conversion rates on all the hcp Ru and fcc Ru facets. The calculated equilibrium constant, reaction rate constant, reaction rate and conversion rate for all the facets considered are

DOI:10.1063/1674-0068/cjcp2009171 ©2020 Chinese Physical Society

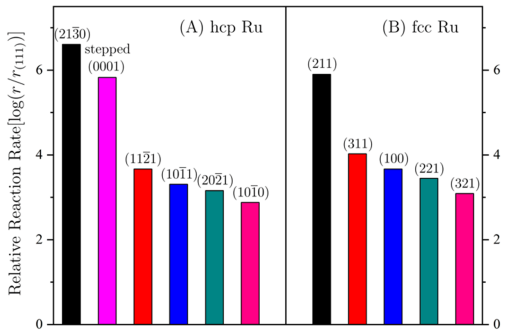

FIG. 7 Relative reaction rate for N_2 dissociation on hcp Ru and fcc Ru surfaces at T=700 K, P=100 bar. All rates r are normalized by that of fcc Ru (111) surface with units of molecule·site^{-1}·s^{-1}.

listed in Table III for hcp Ru and fcc Ru. N_2 dissociation rate is structure-sensitive and determined by N_2 adsorption energies and activation barriers. N_2 dissociation rate (r) varies from 6.8×10^{-4} site^{-1}·s^{-1} to 4.7×10^{5} site^{-1}·s^{-1} and from 1.2×10^{1} site^{-1}·s^{-1} to 9.1×10^{4} site^{-1}·s^{-1} among all the facets exposed in hcp Ru and fcc Ru Wulff shapes, respectively. For hcp Ru, the (21$\bar{3}$0) facet has the highest reaction rate (4.7×10^{5} site^{-1}s^{-1}) which is at least three orders of magnitude higher than other facets. Whereas, the stepped hcp Ru (0001) surface has the second highest N_2 activation rate (7.7×10^{4} site^{-1}·s^{-1}). N_2 dissociation rates for the remaining facets decrease following the sequence: (11$\bar{2}$1) (5.4×10^{2} site^{-1}·s^{-1}), (10$\bar{1}$1) (2.4×10^{2} site^{-1}·s^{-1}), (20$\bar{2}$1) (1.7×10^{2} site^{-1}·s^{-1}), (10$\bar{1}$0) (8.7×10^{1} site^{-1}·s^{-1}), (10$\bar{1}$2) (4.4 site^{-1}·s^{-1}) and (0001) (6.8×10^{-4} site^{-1}·s^{-1}). For fcc Ru, the stepped (211) facet has the largest reaction rate of 9.1×10^{4} site^{-1}·s^{-1}; (311), (100) and (221) surfaces have very similar reaction rates ranging from 1.2×10^{3} site^{-1}·s^{-1} to 3.3×10^{2} site^{-1}·s^{-1}. However, (321) and (111) surfaces are less active for N_2 dissociation with the reaction rates of 1.4×10^{2} site^{-1}·s^{-1} and 1.2×10^{-1} site^{-1}·s^{-1}, respectively.

Taking into account the number of the active sites of a specific facet, we gave the conversion rate of each facet exposed in the hcp Ru and fcc Ru Wulff shapes except for the stepped hcp Ru (0001). From Table III, we can see that the conversion rate follows the sequence by (21$\bar{3}$0)>(10$\bar{1}$1)>(10$\bar{1}$0)>(11$\bar{2}$1)>(20$\bar{2}$1)>(10$\bar{1}$2)>(0001) for hcp Ru varying from 1.5×10^{22} s^{-1} to 1.9×10^{15} s^{-1}, whereas (211)>(311)>(100)>(221)>(321)>(111) for fcc Ru varying from 2.0×10^{22} s^{-1} to 1.2×10^{18} s^{-1}. To see N_2 dissociation activity intuitively, the relative reaction rate of hcp Ru and fcc Ru facets referring to the reaction rate value of fcc (111) are also plotted in FIG. 7. For hcp Ru, although (21$\bar{3}$0) surface has a small surface area ratio (1%), the lowest activation barrier of N_2 dissociation results in the highest N_2 conversion rate of 1.5×10^{22} s^{-1}, which is a major contribution to the total conversion rate of hcp Ru. The conversion rate for (10$\bar{1}$1) surface, which has the largest surface area, becomes only 9.5×10^{20} s^{-1}, nearly the same as that for fcc Ru (311) surface. Meanwhile, fcc Ru (211) surface has the highest N_2 conversion rate of 2.0×10^{22} s^{-1}, which are more than two orders higher than that of all the other fcc Ru surfaces.

By summarizing all the contributions of each facets, the calculated total conversion rate of fcc Ru for N_2 activation becomes 2.2×10^{22} s^{-1} *vs.* 1.6×10^{22} s^{-1} to that of hcp Ru even considering the most active hcp Ru {21$\bar{3}$0} facet. Given that when hcp Ru particle size is decreasing, hcp Ru {21$\bar{3}$0} surface will not be able to expose owing to its high surface energy. Therefore, fcc Ru is apparently more active than hcp Ru for N_2 activation due to the exposure of abundant step and edge sites on {211} surface. Additionally, there are eight {111} surfaces exposed in the Wulff shape of fcc Ru, while the Wulff shape of hcp Ru is covered by two {0001} surfaces. The step sites can form at the edge of flat surfaces and more monatomic step sites exposed in fcc Ru can enhance N_2 dissociation activity further.

Based on our DFT calculation studies, we propose here possible ways to design highly active Ru-based catalyst for ammonia synthesis. Fcc Ru catalyst should be synthesized to enhance N_2 dissociation activity by increasing the exposure of more {211} facets and step sites. Even for hcp Ru, there is still much room for improving the activity of N_2 activation by the usage of the highly active monatomic stepped sites on or at the edge of hcp Ru {0001} surface. Our work agrees well with the previous studies by Nørskov *et al.* that the stepped site on hcp Ru {0001} surface is considered as the active site for the ammonia synthesis process [16, 26, 72, 73].

Our previous DFT calculations indicated that hcp Co has higher N_2 dissociation activity than fcc Co due to the denser active sites with high intrinsic activity in hcp Co Wulff shape [56]. In principle, Ru is more active than Co for N_2 activation due to the lower activation barriers for N_2 dissociation on Ru. The difference between Co and Ru is that fcc Ru exhibits better performance than hcp Ru for N_2 activation. This can be attributed to the fact that Ru has larger lattice constants than Co [74], which results in different transition state configurations over the facets of Ru compared to Co.

IV. CONCLUSION

DFT calculations were performed to study the structure sensitivity of N_2 activation on hcp Ru and fcc Ru. First-principles kinetic study indicates that {21$\bar{3}$0} facet has the highest activity for N_2 activation in hcp Ru, followed by the monatomic step sites. Whereas the stepped {211} facet achieves best performance for N_2 activation in fcc Ru. Fcc Ru is more active than hcp Ru for N_2 conversion, which can be understood by the exposure of more active sites over the stepped {211} facet

DOI:10.1063/1674-0068/cjcp2009171 ©2020 Chinese Physical Society

and monatomic step in fcc Ru. Our work provides a pragmatic way to improve the mass-specific activity of N_2 dissociation by using fcc Ru catalysts.

V. ACKNOWLEDGMENTS

This work was supported by the National Natural Science Foundation of China (No.91645202 and No.91945302), the Key Technologies R&D Program of China (2017YFB0602205 and 2018YFA0208603), the Chinese Academy of Sciences Key Project (QYZDJ-SSW-SLH054); and the Super Computing Center of USTC is gratefully acknowledged.

[1] J. W. Erisman, M. A. Sutton, J. Galloway, Z. Klimont, and W. Winiwarter, Nat. Geosci. **1**, 636 (2008).
[2] J. G. Chen, R. M. Crooks, L. C. Seefeldt, K. L. Bren, R. M. Bullock, M. Y. Darensbourg, P. L. Holland, B. Hoffman, M. J. Janik, A. K. Jones, M. G. Kanatzidis, P. King, K. M. Lancaster, S. V. Lymar, P. Pfromm, W. F. Schneider and R. R. Schrock, Science **360**, eaar6611 (2018).
[3] D. E. Brown, T. Edmonds, R. W. Joyner, J. J. McCarroll, and S. R. Tennison, Catal. Lett. **144**, 545 (2014).
[4] I. Chorkendorff and J. W. Niemantsverdriet, *Concepts of Modern Catalysis and Kinetics*, John Wiley & Sons, 301 (2003).
[5] N. Spencer, R. Schoonmaker, and G. Somorjai, J. Catal. **74**, 129 (1982).
[6] D. R. Strongin and G. A. Somorjai, J. Catal. **109**, 51 (1988).
[7] J. J. Mortensen, L. B. Hansen, B. Hammer, and J. K. Norskov, J. Catal. **182**, 479 (1999).
[8] S. Hagen, R. Barfod, R. Fehrmann, C. J. H. Jacobsen, H. T. Teunissen, and I. Chorkendorff, J. Catal. **214**, 327 (2003).
[9] T. Kandemir, M. E. Schuster, A. Senyshyn, M. Behrens, and R. Schlögl, Angew. Chem. Int. Ed. **52**, 12723 (2013).
[10] G. Ertl, H. Knözinger, and J. Weitkamp, *Handbook of Heterogeneous Catalysis*, Weinheim: Wiley-VCH, 2965 (2008).
[11] K. I. Aika, H. Hori, and A. Ozaki, J. Catal. **27**, 424 (1972).
[12] S. Dahl, J. Sehested, C. Jacobsen, E. Törnqvist, and I. Chorkendorff, J. Catal. **192**, 391 (2000).
[13] S. Dahl, E. Törnqvist, and I. Chorkendorff, J. Catal. **192**, 381 (2000).
[14] N. Saadatjou, A. Jafari, and S. Sahebdelfar, Chem. Eng. Commun. **202**, 420 (2015).
[15] X. Wang, J. Ni, B. Lin, R. Wang, J. Lin, and K. Wei, Catal. Commun. **12**, 251 (2010).
[16] Á. Logadóttir and J. K. Nørskov, J. Catal. **220**, 273 (2003).
[17] H. Liu, Chin. J. Catal. **35**, 1619 (2014).
[18] K. Honkala, A. Hellman, I. N. Remediakis, A. Logadottir, A. Carlsson, S. Dahl, C. H. Christensen, and J. K. Nørskov, Science **307**, 555 (2005).
[19] A. Ozaki, H. S. Taylor, and M. Boudart, Proc. Math. Phys. Sci. **258**, 47 (1960).
[20] A. Nielsen, J. Kjaer, and B. Hansen, J. Catal. **3**, 68 (1964).
[21] M. Boudart, Cat. Rev. **23**, 1 (1981).
[22] K. Tamaru, Acc. Chem. Res. **21**, 88 (1988).
[23] H. Tanaka, Y. Nishibayashi, and K. Yoshizawa, Acc. Chem. Res. **49**, 987 (2016).
[24] H. Grabke, W. Paulitschke, G. Tauber, and H. Viefhaus, Surf. Sci. **63**, 377 (1977).
[25] M. Grunze, M. Golze, W. Hirschwald, H. J. Freund, H. Pulm, U. Seip, M. Tsai, G. Ertl, and J. Küppers, Phys. Rev. Lett. **53**, 850 (1984).
[26] S. Dahl, A. Logadottir, R. C. Egeberg, J. H. Larsen, I. Chorkendorff, E. Tornqvist, and J. K. Nørskov, Phys. Rev. Lett. **83**, 1814 (1999).
[27] C. J. H. Jacobsen, S. Dahl, P. L. Hansen, E. Törnqvist, L. Jensen, H. Topsøe, D. V. Prip, P. B. Møenshaug, and I. Chorkendorff, J. Mol. Catal. A: Chem. **163**, 19 (2000).
[28] W. Raróg-Pilecka, E. Miśkiewicz, D. Szmigiel, and Z. Kowalczyk, J. Catal. **231**, 11 (2005).
[29] A. Hellman, K. Honkala, S. Dahl, C. H. Christensen, and J. K. Nørskov, *Comprehensive Inorganic Chemistry II (2nd Edn.)*, Amsterdam: Elsevier, 459 (2013).
[30] R. Van Hardeveld and F. Hartog, Surf. Sci. **15**, 189 (1969).
[31] Y. K. Kim, G. A. Morgan, and J. T. Yates, Surf. Sci. **598**, 14 (2005).
[32] S. Shetty and R. A. van Santen, Top. Catal. **53**, 969 (2010).
[33] C. A. Casey-Stevens, S. G. Lambie, C. Ruffman, E. Skúlason, and A. L. Garden, J. Phys. Chem. C **123**, 30458 (2019).
[34] S. Liang, F. Teng, G. Bulgan, R. Zong, and Y. Zhu, J. Phys. Chem. C **112**, 5307 (2008).
[35] M. T. M. Koper, Nanoscale **3**, 2054 (2011).
[36] K. Kusada, H. Kobayashi, T. Yamamoto, S. Matsumura, N. Sumi, K. Sato, K. Nagaoka, Y. Kubota, and H. Kitagawa, J. Am. Chem. Soc. **135**, 5493 (2013).
[37] E. K. Abo-Hamed, T. Pennycook, Y. Vaynzof, C. Toprakcioglu, A. Koutsioubas, and O. A. Scherman, Small **10**, 3145 (2014).
[38] J. Gu, Y. Guo, Y. Y. Jiang, W. Zhu, Y. S. Xu, Z. Q. Zhao, J. X. Liu, W. X. Li, C. H. Jin, C. H. Yan, and Y. W. Zhang, J. Phys. Chem. C **119**, 17697 (2015).
[39] H. Ma and C. Na, ACS Catal. **5**, 1726 (2015).
[40] S. I. Choi, J. A. Herron, J. Scaranto, H. Huang, Y. Wang, X. Xia, T. Lv, J. Park, H. C. Peng, M. Mavrikakis, and Y. Xia, ChemCatChem **7**, 2077 (2015).
[41] J. X. Liu, B. Y. Zhang, P. P. Chen, H. Y. Su, and W. X. Li, J. Phys. Chem. C **120**, 24895 (2016).
[42] N. M. AlYami, A. P. LaGrow, K. S. Joya, J. Hwang, K. Katsiev, D. H. Anjum, Y. Losovyj, L. Sinatra, J. Y. Kim, and O. M. Bakr, Phys. Chem. Chem. Phys. **18**, 16169 (2016).
[43] H. Ye, Q. Wang, M. Catalano, N. Lu, J. Vermeylen, M. J. Kim, Y. Liu, Y. Sun, and X. Xia, Nano Lett. **16**, 2812 (2016).
[44] Y. Yao, D. S. He, Y. Lin, X. Feng, X. Wang, P. Yin, X. Hong, G. Zhou, Y. Wu, and Y. Li, Angew. Chem. **128**, 5591 (2016).
[45] Z. Fan and H. Zhang, Acc. Chem. Res. **49**, 2841 (2016).

DOI:10.1063/1674-0068/cjcp2009171 ©2020 Chinese Physical Society

[46] W. Z. Li, J. X. Liu, J. Gu, W. Zhou, S. Y. Yao, R. Si, Y. Guo, H. Y. Su, C. H. Yan, W. X. Li, Y. W. Zhang, and D. Ma, J. Am. Chem. Soc. **139**, 2267 (2017).
[47] Y. Yu, G. H. Nam, Q. He, X. J. Wu, K. Zhang, Z. Yang, J. Chen, Q. Ma, M. Zhao, Z. Liu, F. R. Ran, X. Wang, H. Li, X. Huang, B. Li, Q. Xiong, Q. Zhang, Z. Liu, L. Gu, Y. Du, W. Huang, and H. Zhang, Nat. Chem. **10**, 638 (2018).
[48] X. Hao, R. Zhang, L. Ling, M. Fan, D. Li, and B. Wang, J. Phys. Chem. C **124**, 6756 (2020).
[49] M. Zhao and Y. Xia, Nat. Rev. Mater. **5**, 440 (2020).
[50] A. Y. Khodakov, Catal. Today **144**, 251 (2009).
[51] M. Sadeqzadeh, H. Karaca, O. Safonova, P. Fongarland, S. Chambrey, P. Roussel, A. Griboval-Constant, M. Lacroix, D. Curulla-Ferré, and F. Luck, Catal. Today **164**, 62 (2011).
[52] D. Song, J. Li, and Q. Cai, J. Phys. Chem. C **111**, 18970 (2007).
[53] O. Ducreux, J. Lynch, B. Rebours, M. Roy, and P. Chaumette, Stud. Surf. Sci. Catal. **119**, 125 (1998).
[54] O. Ducreux, B. Rebours, J. Lynch, M. Roy-Auberger, and D. Bazin, Oil Gas Sci. Technol. **64**, 49 (2009).
[55] J. X. Liu, H. Y. Su, D. P. Sun, B. Y. Zhang, and W. X. Li, J. Am. Chem. Soc. **135**, 16284 (2013).
[56] B. Y. Zhang, P. P. Chen, J. X. Liu, H. Y. Su, and W. X. Li, J. Phys. Chem. C **123**, 10956 (2019).
[57] M. Zhao, L. Figueroa-Cosme, A. O. Elnabawy, M. Vara, X. Yang, L. T. Roling, M. Chi, M. Mavrikakis, and Y. Xia, Nano Lett. **16**, 5310 (2016).
[58] G. Kresse and J. Hafner, Phys. Rev. B **47**, 558 (1993).
[59] G. Kresse and J. Furthmüller, Phys. Rev. B **54**, 11169 (1996).
[60] G. Kresse and D. Joubert, Phys. Rev. B **59**, 1758 (1999).
[61] J. P. Perdew, K. Burke, and M. Ernzerhof, Phys. Rev. Lett. **77**, 3865 (1996).
[62] M. Methfessel and A. T. Paxton, Phys. Rev. B **40**, 3616 (1989).
[63] K. H. Hellwege, A. M. Hellwege, B. Eisenmann, and H. Schaefer, *Structure Data of Elements and Intermetallic Phases*, Berlin: Springer-Verlag, (1971).
[64] C. Song, O. Sakata, L. S. R. Kumara, S. Kohara, A. Yang, K. Kusada, H. Kobayashi, and H. Kitagawa, Sci. Rep. **6**, 31400 (2016).
[65] K. Sun, Y. Zhao, H. Y. Su, and W. X. Li, Theor. Chem. Acc. **131**, 1118 (2012).
[66] G. Henkelman, B. P. Uberuaga, and H. Jónsson, J. Chem. Phys. **113**, 9901 (2000).
[67] G. Wulff and Z. Kristallogr. Cryst. Mater. **34**, 449 (1901).
[68] H. Lin, J. X. Liu, H. Fan, and W. X. Li, J. Phys. Chem. C **124**, 11005 (2020).
[69] J. X. Liu and W. X. Li, WIREs Comput. Mol. Sci. **6**, 571 (2016).
[70] P. Crawford and P. Hu, J. Phys. Chem. B **110**, 24929 (2006).
[71] D. R. Stull, JANAF Thermochem. Tables. Clearinghouse, (1965).
[72] T. H. Rod, A. Logadottir, and J. K. Nørskov, J. Chem. Phys. **112**, 5343 (2000).
[73] R. Schlögl, Angew. Chem. Int. Ed. **42**, 2004 (2003).
[74] N. Ashcroft and N. Mermin, *Solid State Physics*, Philadelphia: Saunders College (1976).

DOI:10.1063/1674-0068/cjcp2009171 ©2020 Chinese Physical Society